Intramolecular and Intermolecular Rearrangements in Nanoconfined Polystyrene

Sudeshna Chattopadhyay,[†] Alokmay Datta,*[,†] A. Giglia,[‡] N. Mahne,[‡] A. Das,[†] and S. Nannarone[‡]

Surface Physics Division, Saha Institute of Nuclear Physics, 1/AF, Bidhannagar, Kolkata 700 064, India, and TASC-INFM, AREA Science Park, S.S. 14 Km 163.5, I-34012, Basovizza (TS), Italy

Received June 22, 2007; Revised Manuscript Received October 4, 2007

ABSTRACT: Vacuum ultraviolet spectroscopy reveals an intramolecular rearrangement involving a change in "physical dimers" of adjacent pendant benzene rings of atactic polystyrene (aPS) from "oblique" to "head-to-tail" (ht) configuration in aPS films spin coated on fused quartz, as film thickness R goes below $4R_g$ (R_g = unperturbed polystyrene gyration radius ≈ 20.4 nm). Simultaneously, transverse layering of molecular "gyration spheres", for film thickness $R \leq 4R_g$, causes an increase in free energy (reduction in cohesion) that follows a $(R_g/R)^b$ dependence with $b \approx 3$, a clear deviation from planar confinement. The variation of in-plane and out-of-plane cohesive energy over a film of a given thickness is explained by invoking a fixed-range, repulsive, modified Pöschl-Teller intermolecular potential, with the strength of this potential decreasing with increase in R. Possible reduction of "dimer" dipole moment due to ht configuration is consistent with reduction of cohesion between aPS molecular gyration spheres.

Introduction

Despite of considerable interest over the years in applications of polymers with controlled electrical and mechanical properties, the nature of the electronic states in macromolecules such as polymers[1−9] and DNA[10] remains a subject of controversy. The central issue is whether these states, localized or extended in character, are dependent on the molecular conformation of the polymer.[1−5] In this context, pendant-group polymers are very interesting from a theoretical point of view, since π-electrons reside on these pendant groups and there is generally no conjugation path along backbone of the chain. Polystyrene constitutes a prototype for the class of pendant-group polymers. These materials, which have a wide range of practical applications, consist of a saturated backbone (C−C−) on which aromatic side groups (phenyl groups) are attached. Polymers with a unique way of coupling of the monomer units are called isotactic and are contrasted to those with an irregular steric structure, which are addressed as atactic. If the coupling varies, but in a regular way, polymer chains are called syndiotactic. All three types are found for polystyrene, depending on the process chosen for the synthesis.[11] Atactic polystyrene (aPS) is believed not to crystallize, because of its lack of stereoregularity, and is considered as an amorphous polymer.

However, a study of the very intense pure electronic singlet $^1A_{1g} \rightarrow {}^1E_{1u}$ of polystyrene as a part of vacuum ultraviolet spectroscopy[5,12] (vuv) shows a large shift of the polystyrene peak from 6.566 eV (189 nm) in solution to about 6.3 eV (197 nm) in solid phase, which is larger than that which would be expected from solvent effects alone and hence an exciton-type interaction between the benzene groups of the polymer chain seems possible.[5] Moreover, the blue shift of this transition within the confinement of polystyrene solid film[12] supports the exciton-type interaction in the benzene groups, which also indicates some correlated spatial arrangement between the pendant benzene rings in polystyrene solid film. It was also observed from dielectric relaxation spectroscopy that, besides the known α-relaxation, two additional relaxation processes β_1 and β_2 were present in various samples of unannealed aPS and syndiotactic polystyrene (sPS) films spin cast from solvent solutions.[13] These new dynamic processes, not found in bulk aPS samples, show Arrhenius behavior, common activation energy around 80 kJ mol^{-1}, and cross the α-relaxation region without merging. This observation indicates coexistence of two phases, one amorphous and the other nonamorphous, with specific structural and dynamic properties. From studies on sPS films and bulk, β_1 and β_2 processes are known to be dielectric manifestations of local fluctuations within helical "rods" formed by syndiotactic sequences. Though the relaxation strength for these processes is slightly different for aPS and sPS, the fact that they are at all present in aPS films and moreover have the same activation energy points to a common inter- or intramolecular potential involved in both fluctuations.[13] More interestingly, existence of such nonamorphous conformations inside these unannealed aPS films was confirmed by FTIR measurements.[13] In the FTIR spectra of polystyrene, bands in the 500−600 cm^{-1} region correspond to out-of-plane deformation of benzene ring and are conformation sensitive to the T_2G_2 helix sequences.[14,15] The two peaks at 548 and 572 cm^{-1}, known to be characteristic of helix conformation, appear for both aPS (spin cast from toluene solutions) and sPS and are absent in a bulk sample of the pure aPS.[13]

These studies thus indicate a conformational change, i.e., an intramolecular rearrangement in spin-cast polystyrene films, which (i) has nonamorphous or stereoregular features, (ii) involves the pendant benzene rings (or phenyl groups), and (iii) is absent in bulk samples. This confinement-induced intramolecular rearrangement finds an echo in the intermolecular ordering observed in films of fluids, including polymers. One-dimensional geometrical confinement in films causes the fluid

* To whom correspondence should be addressed. E-mail: alokmay.datta@saha.ac.in. Phone: 91-033-2337-5345, extn 4216. FAX: 91-033-2337-4637.

[†] Saha Institute of Nuclear Physics.

[‡] TASC-INFM.

10.1021/ma071392y CCC: $37.00
Published on Web 11/15/2007

to form layers normal to the confinement direction.[16−18] For such "nanoconfined" simple fluids, the layer periodicity is equal to the molecular size, while for polymers, it is equal to the unperturbed gyration radius (R_g), i.e., the dimension of a polymer molecule in the maximum entropy configuration.[19] Nanoconfined fluids exhibit radically new mechanical, thermal, dielectric, and rheological properties.[20−22] In a recent study, a nanoconfined simple liquid has been observed to be in a "laterally cooperative" state that behaves liquidlike or solidlike depending on the kinematics of the measurement process.[23] In polymers, layers form only when the film thickness is less than $4R_g$ and there is a measurable reduction in cohesion between adjacent molecular gyration spheres,[12] as predicted by theoretical studies,[24] along the film thickness. Tapping-mode atomic force microscopy (TM-AFM) studies reveal a confinement-induced reduction in cohesion between adjacent molecular gyration spheres on film surface (in-plane),[25] which is very similar to the cohesion reduction along the film thickness (out-of-plane).[12] A confinement-induced reduction in cohesion had also been suggested from experiments on complex fluids.[26] These new properties suggest a connection between intra- and intermolecular reorganization in complex fluids under confinement that is bound to have strong implications in any technology employing thin fluid films such as optoelectronic and magnetic coatings, adhesives, biological membranes, and emerging nanotechnologies, in particular, photonics and nanofluidis.

In this communication, we present the results of our studies on intramolecular and intermolecular rearrangements in nanoconfined polystyrene. Specifically, we show from vuv spectroscopy that, in spin-cast aPS films on fused quartz, reduction in film thickness below $4R_g$ leads to a configurational change in correlated pairs of pendant benzene rings (physical dimers) from oblique (ob) to head-to-tail (ht), which indicates a reduction of dimer dipole moment to near zero. Coming to intermolecular rearrangements, we have already found from our previous studies, using X-ray reflectivity (XRR) and TM-AFM techniques, confinement-induced reduction in cohesion between adjacent molecular gyration spheres along the film thickness (out-of-plane)[12] and on the film surface (in-plane).[25] We will show here that these out-of-plane and in-plane reductions of cohesion energy are very similar in nature for a given nanoconfined film, i.e., film thickness $R \leq 4R_g$. We have explained this drop in cohesion by the emergence of a new, repulsive intermolecular potential that fits well with a modified Pöschl-Teller potential (MPT),[27] the depth of which can be increased by thinning the film but the range is invariant with confinement. We have also observed that an increase in free energy due to nanoconfinement does not tally with that observed for planar confinement.[28,29] We show that the intermolecular repulsive potential, which explains lowering of cohesion, increases as $(R_g/R)^3$ whereas the benzene dimer dihedral angle suddenly decreases as the aPS film thickness becomes less than $4R_g$.

The organization of the paper is as follows. In the present section, we introduce our research perspective and motivation. In the next section, we describe the preparation of aPS films of different thicknesses (R-values) and the various experimental procedures and data analysis schema used by us. The Results and Discussions section has been divided into two subsections. In the first subsection, we present our measurements using vuv spectroscopy and show the change in configuration of benzene dimers in an aPS film as film thickness (R) becomes less than $4R_g$. In other words, we demonstrate a confinement-induced intramolecular rearrangement in aPS film. In the second subsection, we present our measurements using TM-AFM and the surface free energy (cohesive energy) variations extracted from the phase images as well as XRR measurements and electron density profiles (EDPs), i.e., the variation of polymer electron density along the film thickness obtained from these measurements and, in turn, variations of out-of-plane cohesive energy (free energy) provided by these EDPs. Here we also show the dependence of increase in free energy due to confinement on polystyrene film thickness and that this increase does not show a planar confinement-like behavior. Then, from variations in cohesive energy along the film surface and film thickness, we invoke a new intermolecular potential that behaves like a MPT potential and show that the strength of this potential depends on film thickness, while the range is fixed. The last section presents conclusions and outlook.

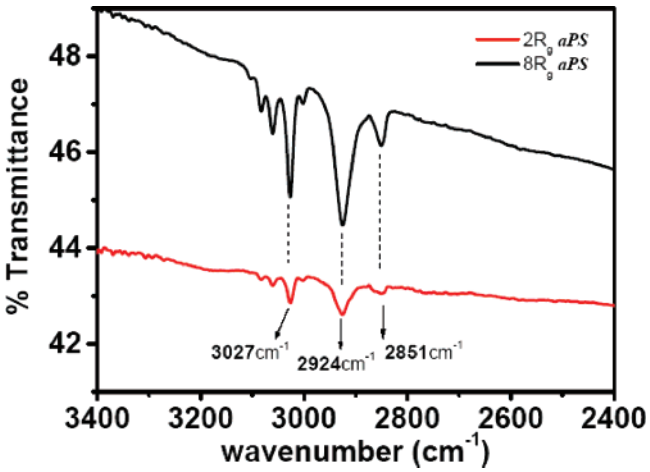

Figure 1. FTIR spectra (transmittance vs wavenumber) of $2R_g$ (≈40 nm) and $8R_g$ (≈160 nm) thick aPS films. The strong absorption peaks are assigned as follows: methylene symmetric stretch = 2851 cm^{-1}, methylene asymmetric stretch = 2924 cm^{-1}, and aromatic hydrocarbon stretch = 3027 cm^{-1}.

Experimental Section

Atactic PS ($M_w \approx 560900$, $R_g = 0.272M_w^{1/2} \approx 20.4$ nm, $M_w/M_n = 1.01$, where M_w and M_n are the weight average and number average molecular weights)[30] was spin coated on fused quartz plates from toluene solutions using a photoresist spin coater (Headway Inc.) to form films with R varying from 40 (≈$2R_g$) to 147 nm (≈$7R_g$) and with air/film and film/substrate interfacial roughness of ∼0.6 nm, as has been described previously.[12] Before the start of experiments with spin-cast aPS films, Fourier transform infrared (FTIR) spectroscopic analysis using a Spectrum GX Perkin-Elmer spectrometer was carried out on the films. As shown in Figure 1, all characteristic peaks of polystyrene in this range were present.[31] However, no peak was present in either the 2870−2890 cm^{-1} or the 2950−2970 cm^{-1} range, which contain, respectively, the (strong) symmetric and asymmetric stretch bands of the methyl group[31] of toluene contaminant. Absence of any absorption peak in this range thus rules out the presence of toluene in our aPS films. Contaminants were removed from the substrate by boiling it in 5:1:1 $H_2O/H_2O_2/NH_4OH$ solution for 10 min followed by rinsing in acetone and ethyl alcohol. All data were collected at room temperature and, except for vuv spectra, at ambient pressure.

Grazing incidence X-ray reflectivity data of aPS films with $R_g \leq R \leq 8Rg$ were collected using an 18 kW rotating anode X-ray generator (Enraf Nonius FR591). The Cu $K\alpha_1$ line at $\lambda = 0.1540562$ nm was selected with a Si(111) monochromator, and measurements were carried out in a triple-axis diffractometer (Optix Microcontrole). Specular reflectivity scans, i.e., scans in the plane containing the incident beam and normal to the sample surface, with incident angle α_{in} = scattering angle α_{sc}, were performed with α_{in} varying

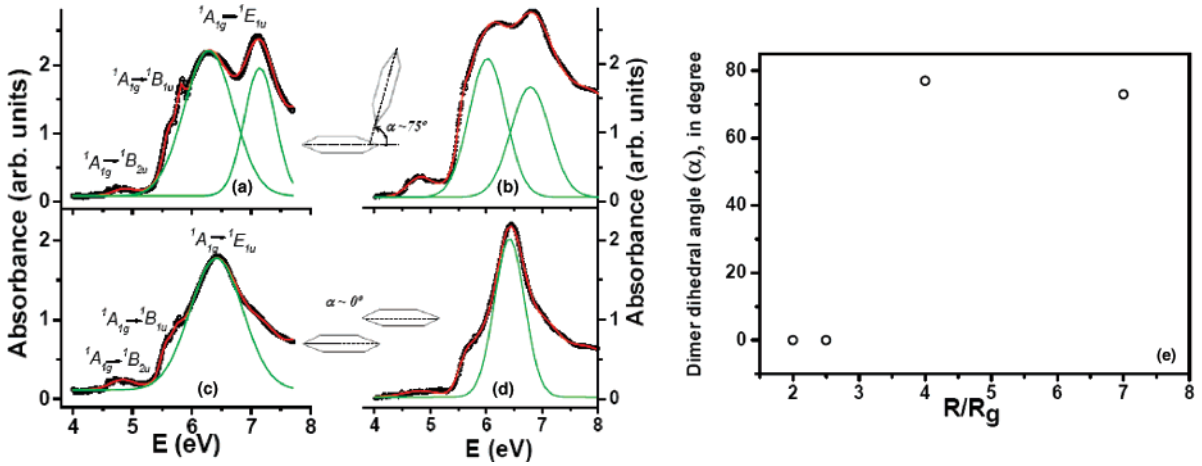

Figure 2. Transmission spectra (absorbance vs photon energy in electronvolts) in vacuum ultraviolet (vuv) for aPS films with film thicknesses R = 147.0 nm (a), 84.0 nm (b), 50.0 nm (c), and 40.0 nm (d): circles, data; red line, convolution of individual Gaussian fits (only those for dimer peaks are shown in green). Assigned transitions are presented besides the spectral bands for representative spectra (a) and (c). Configurations of benzene dimers in polystyrene extracted from the analysis of $^1A_{1g} \rightarrow {}^1E_{1u}$ are shown in insets in upper and lower panels (α = dimer dihedral angle). See text for details. (e) Plot of α vs R/R_g.

from 0° to 3° in 5 mdeg steps. If $\mathbf{q} = \mathbf{k}_s - \mathbf{k}_i$ is the momentum transfer vector, with $\mathbf{k}_{s(i)}$ being the scattered (incident) X-ray wave vector, then this geometry makes the components in the sample plane, $q_x = q_y = 0$, and the value of q_z (=$(4\pi/\lambda)$ sin α_{in}), the component normal to the sample surface, vary from 0 to 4.3 nm^{-1}. The resolution in q_z is $\cong 2.9 \times 10^{-3}$ nm^{-1}, and the spatial resolution along the film depth is given by $2\pi/q_z^{max}$, where q_z^{max} is the maximum value of q_z to which Kiessig fringes are observed. In our experiments this gives a typical value of $\cong$1.5 nm for z resolution.

We have analyzed our reflectivity data using the scheme of distorted wave Born approximation (DWBA),[32] which treats the film as a perturbing potential causing the scattering. This method is very sensitive to small density variations and has been used to detect density variations due to layering in liquids or polymers.[16,17] Variations of ρ are expected to be small in aPS films, and following our previous studies, we have used the DWBA method to extract EDPs for these films and to look for layer formation. In this scheme, we consider the film to be composed of a number of slices of equal thickness with electron density $\rho(z) = \rho_0 + \Delta\rho(z)$, where $\Delta\rho$ varies with slices but is constant in a slice. The specular reflectivity is then given by:[17]

$$\mathcal{R}(q_z) = |ir_0(q_z) + (4\pi r_e/q_z)[a_t^2(q_z)\Delta\rho(q_z) + a_r^2(q_z)\Delta\rho^*(q_z)]|^2 \quad (1)$$

where r_0 is the specular reflectance coefficient of the average film of electron density ρ_0, a_t and a_r are the coefficients for transmitted and reflected amplitudes of the average film, and $\Delta\rho(q_z)$ is the Fourier transform of $\Delta\rho(z)$. By selection of a sufficient number of slices (of width always greater than 1.5 nm, the maximum achievable resolution) and an appropriate ρ_0 for the film, we fit eq 1 after required convolution of the calculated reflectivity for the detector slit (with a Gaussian width of 400 μm) to the data for aPS films, keeping $\Delta\rho$'s and air/PS and PS/Qtz Gaussian interface widths (σ_{PS} and σ_{PS-Qtz}) as the fit parameters. The EDP is constructed from the values of $\rho(z)$ obtained from the best fit. The veracity of this procedure has been crosschecked by generating the reflectivity profiles from the extracted EDPs using the (more general) Parratt scheme.

AFM images were acquired with Nanoscope IV (Veeco Instruments) using etched Si tip and phosphorus doped Si cantilevers. We have worked in the tapping mode with A_0, the free amplitude of the cantilever = 36 nm, A, the set point amplitude = 10.94 nm, ω_0, the resonance frequency = $2\pi \times 283$ kHz, Q, the quality factor = 505, and k, the cantilever spring constant = 20 N/m. Both topographic and phase images have been collected for aPS samples. We have estimated the average energy, E_D, dissipated per cycle by the tip over the film surfaces, from the phase images, using the expression[33]

$$\sin\phi = \left(\frac{\omega}{\omega_0}\frac{A}{A_0}\right) + \frac{QE_D}{\pi kAA_0} \quad (2)$$

where ϕ is the phase shift with respect to the drive signal and ω is the working frequency. Tip interaction (during approach and retraction) with the surface via the van der Waals force is modeled as a sphere approaching a plane with an effective contact area $4\pi r_c\alpha_{Si}$, where r_c is the radius of tip curvature and α_{Si} is the Si atom diameter. Then the relative energy dissipation by the tip in film planes with respect to minima is given by[25]

$$\Delta E_D = \frac{2}{3}\frac{r_c\alpha_{Si}}{z_0^2}\Delta A_{SiPS} \quad (3)$$

where we have considered the tip−sample adhesion, given by the corresponding Hamaker constant A_{SiPS}, to be the varying interaction.[34] This is unaffected by cantilever tilt.[35] Here z_0 is the tip−sample separation ($\approx$0.2 nm in contact[2]), $r_c \approx 10$ nm and α_{Si} = 0.22 nm. Variation in PS Hamaker constant in the film plane, ΔA_{PS}, can be determined using $A_{SiPS} = A_{Si}^{1/2}A_{PS}^{1/2}$, eq 2 and 3, and the value of A_{Si}, the Si Hamaker constant.[36] Hence, $\Delta\gamma_{PS}$ (in mJ m^{-2}) $\approx \Delta A_{PS}$ (in J)/(2.1 $\times$ 10^{-21}), the variation in surface energy, is determined.[30] In other words, determination of the in-plane variation of Hamaker constant, ($\Delta A^{(i)}_{PS}$), provided the in-plane variation in cohesion, $\Delta G^{(i)}_{PS-PS}$ (=$\Delta\gamma_{PS}$).

We have carried out vuv spectroscopy of polystyrene films with $R \approx 2R_g$, $3R_g$, $4R_g$, and $7R_g$. Transmission spectra in the 4−9 eV range were collected in 10 meV steps at BEAR beamline of ELETTRA synchrotron, with nearly linearly polarized light (the estimated Stokes parameter $S_1 \approx 0.5$) and the electric field lying in the film plane.[37] Repeated scans of the samples in the vuv region studied showed no change in the spectrum, indicating the stable nature of the sample under irradiation in this energy range for the given experimental conditions. The experimental chamber was maintained at $\sim 10^{-10}$ Torr and all measurements were done at ambient temperature. Our focus was on the pure electronic singlet transition $^1A_{1g} \rightarrow {}^1E_{1u}$ involving the pendant benzene rings of aPS, which is centered at 6 eV.

Results and Discussion

1. Intramolecular Rearrangement. Vacuum ultraviolet spectroscopy of aPS films of thickness $R \geq 4R_g$ shows that there

is pronounced splitting in pure electronic singlet transition $^1A_{1g} \rightarrow {}^1E_{1u}$. This π-electronic transition is associated with the pendant benzene ring in the aPS molecule.[5−9,12,38] The splitting in this transition indicates some orientation of the nearest neighbor benzene rings, with small disorder, in aPS film.[39,40] Splitting into two components, as observed for aPS film of thickness $R \geq 4R_g$ (Figure 2a,b), and disappearance of the high-energy component with confinement, $R < 4R_g$ (Figure 2c,d), correspond to the formation of benzene (pendant phenyl group) physical dimer[39] and its configurational change[39,40] with confinement.

Figures 2 shows this spectral band for 147.0 nm (a), 84.0 nm (b), 50.0 nm (c) and 40.0 nm (d) thick aPS films. The split in the band can be explained as arising from the resonant transfer interaction between correlated clusters of pendant benzene rings, given by

$$|J_\beta| = \Delta\nu/2 \tag{4}$$

where $\Delta\nu$ is the measured split,[39,40] which causes the mixing of the singly excited states of individual pendant benzene rings through their transition dipole moments. In our measurements, $\Delta\nu/2 \approx 428$ meV. The doublet splitting indicates that dimers of benzene rings are involved in these clusters. The intensity ratio of the high-energy (−) and low-energy (+) components of the doublets

$$I_+/I_- = (1 + \cos\alpha)/(1 - \cos\alpha) = \cot^2(\alpha/2) \tag{5}$$

gives α, the angle between the transition dipoles, i.e., the dihedral angle between rings of the dimer.[39]

From the change in intensities of these components, it is clear that the dihedral angle goes from ≈75° to ≈0° as film thickness goes from 147.0 to 40.0 nm, corresponding to an oblique or ob configuration (shown schematically in between panels a and b of Figure 2) and a head-to-tail or ht configuration (shown between panels c and d of Figure 2),[40] respectively. Benzene dimer has a permanent dipole moment only when the rings are nonparallel,[41] and hence the ht dimer will have a near-vanishing dipole moment. This would make it undetectable through standard spectroscopic techniques,[41] and to our knowledge, this is the first direct experimental evidence of this "near-parallel" benzene (pendant phenyl ring) dimer. Reduction in dimer dipole moment due to this configurational change would reduce coupling between gyration spheres containing such dimers.

In Figure 2e, we have plotted α as a function of R/R_g, the polymer film thickness. It is clear that there are two configurations of the dimers, corresponding to two values (≈75° and ≈0°) of the dimer dihedral angle for $R \geq 4R_g$ and $R < 4R_g$, respectively. Thus, thinning the film to $4R_g$ causes a sharp transition in dihedral angle, after which the angle remains unchanged on further confinement of the film. We would now like to investigate any intermolecular rearrangement in the PS films that arises due to confinement.

2. Confinement-Induced Intermolecular Potential and Deviation from Planar Confinement. Figure 3a,b shows the phase images obtained from tapping-mode AFM of two typical aPS films with $R \approx 40.0$ and 84.0 nm, respectively. The topographical images of all these films show roughly spherical features with an average diameter $\approx R_g$[12] corresponding to gyration spheres in the film, where $2R_g$ is the diameter of unperturbed gyration sphere observed in dilute solutions. The frusta (≈0.6 nm high) of these spheres are consistent with the top roughness obtained from X-ray studies. But the phase images show larger variations in phase shifts between adjacent spheres

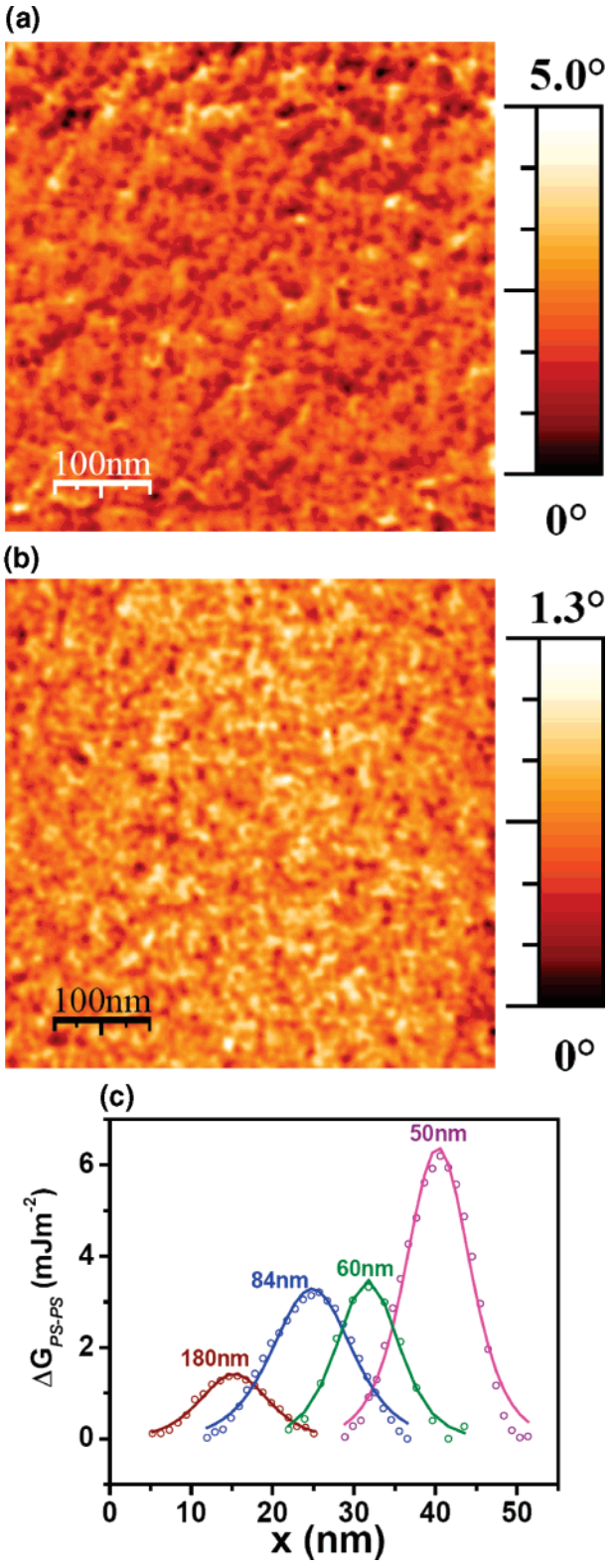

Figure 3. Phase images of tapping-mode AFM scans (500 nm × 500 nm) of PS films with $R = 40.0$ nm ($\approx 2R_g$) (a) and 84.0 nm ($\approx 4R_g$) (b). (c) $\Delta G^{(i)}_{PS-PS}$, variation of cohesion, vs in-plane coordinate x for different R values shown: circles, data; line, best fit with modified Poschl−Teller function. Curves have been side shifted for clarity.

on the film surface as R reduces from 84.0 to 40.0 nm, implying a larger variation in energy dissipated by the AFM tip in going over from sphere to sphere.[33] This again implies a spatial variation in surface free energy over the film with a given thickness, whose magnitude increases with decrease in R. This spatial variation is not observed for $R > 4R_g$, and it cannot be

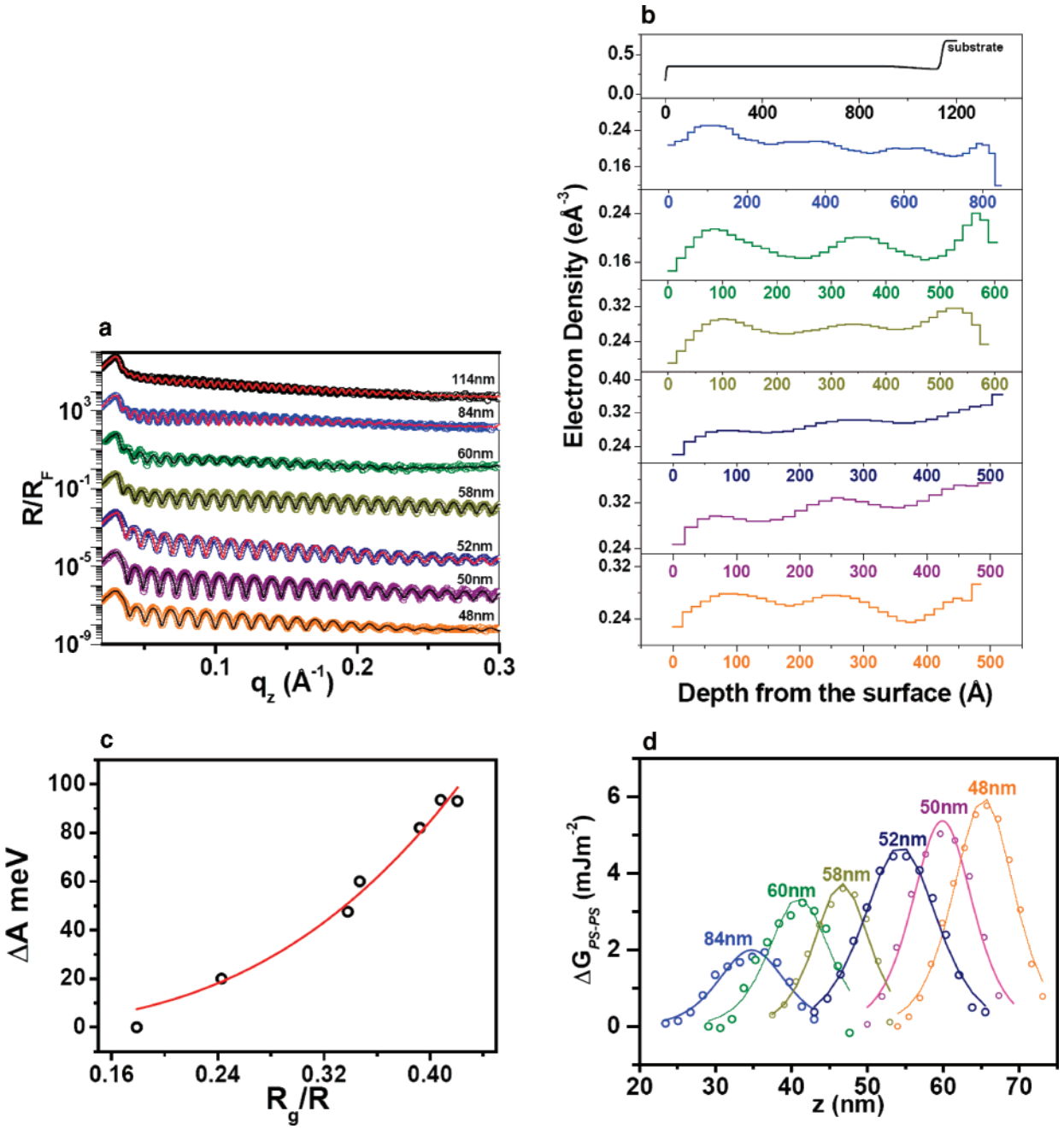

Figure 4. (a) X-ray reflectivity data (circles, Fresnel reflectivity normalized and up shifted) and fits (lines) of PS films on quartz with different thicknesses R (shown beside each curve). (b) Electron density profiles along film depth from reflectivity fits (color coded and presented in same sequence as (a)). (c) $\Delta A^{(o)}_{PS}$, increase in free energy due to layering, vs (R_g/R) (R_g = unperturbed gyration radius of PS, ~20.4 nm): circles, data; line, best fit with $K(R_g/R)^b$. (d) $\Delta G^{(o)}_{PS-PS}$, variation of cohesion, vs depth z for R values shown: circles, data; line, best fit with modified Pöschl-Teller function. Curves have been side shifted for clarity.

explained by simple planar confinement of the polymer. Using the techniques described in the experimental section, we have extracted the reduction of in-plane cohesive energy ($\Delta G^{(i)}_{PS-PS}$). Figure 3c depicts $\Delta G^{(i)}_{PS-PS}$ variation (solid circles) over adjacent gyration spheres as a function of the in-plane coordinate x for different film thicknesses.

Extraction of EDPs along thickness of the film from X-ray reflectivity was obtained using standard methods of analysis, discussed already in the experimental section. Figure 4a shows the reflectivity profiles (open circles) of aPS films of different R values, and the extracted EDPs from the best fit (lines) are shown in Figure 4b in the same sequence and having the same color code. For $R \leq 4R_g$ (~84.0 nm), we observe formation of layers in aPS parallel to the substrate surface, with the error in ρ being an order of magnitude less than this variation.[17] The reduction in cohesive energy caused by the variation of density due to layering is given by[12,30,42]

$$\Delta G^{(o)}_{PS-PS} = -\Delta A^{(0)}_{PS}/(2.1 \times 10^{-21}) \quad (6)$$
$$= -\sigma_{PS}[(\rho(z))^2 - (\rho_{max})^2]/(2.1 \times 10^{-21})$$

where $\Delta G^{(o)}_{PS-PS}$ is the reduction in (out-of-plane) cohesive energy caused by the variation of density due to layering, $\Delta A^{(o)}_{PS}$ is the (out-of-plane) change in polystyrene Hamaker constant, σ_{PS} is the polarizability of aPS, and $\rho(z)$ (ρ_{max}) denotes the electron density at depth z (corresponding maximum).

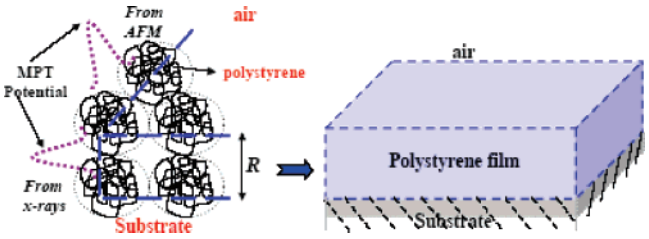

Figure 5. Schematic representation of the confined system showing the modified Pöschl-Teller-like intermolecular potential, as obtained from XRR and AFM.

Table 1. Parameters of the Intermolecular Potential

	peak strength V_0 (mJ m^{-2}) from		range Λ (nm) from	
PS film thickness (nm)	XRR	AFM	XRR	AFM
114	0	1.42	0	5.6
84	1.97	3.29	5.9	6.5
60.4	3.36	3.47	5.3	5.1
58.5	3.73		4.8	
52	4.68		6.4	
50	5.36	6.37	5.3	5.3
48.5	5.95		5.3	

Figure 4c shows the variation of $\Delta A^{(o)}_{PS}$ with R_g/R, obtained from eq 6. The continuous line is the best fit to the data (open circles) with the function:

$$\Delta A^{(o)}_{PS} = K(R_g/R)^b \quad (7)$$

The value of b obtained from this fit is 3.0 ± 0.3. This deviates clearly from $b = 2$ for an ideal polymer or from $b = 1.7$ for a self-avoiding polymer[28] under planar confinement[29] and corresponds to spherical confinement[28] of the polymer. Thus, above a certain degree of confinement, the very nature of confinement is changed by the formation of layers. This is consistent with the three-dimensional variation of cohesion in the nanoconfined polymer, as observed from AFM and X-ray probes discussed above.

Figure 4d shows the observed variation (in solid circles) of $\Delta G^{(o)}_{PS-PS}$ with depth z across the gap between adjacent layers for all the different R-values probed, as shown for $\Delta G^{(i)}_{PS-PS}$ in Figure 3c. In both cases, the abscissa has been shifted arbitrarily for clarity. It is of interest to note that in all cases the values of ΔG_{PS-PS} have a form that fits very well with the modified Pöschl−Teller (MPT) potential given by:[27]

$$\Delta G_{PS-PS}(\xi) = V_0 \cosh^{-2} \alpha'\xi = g^2\alpha'^2 \cosh^{-2} \alpha'\xi \quad (8)$$

Here V_0 is the peak strength of the repulsive intermolecular potential, which has a quadratic dependence on $\alpha' = \Lambda^{-1}$, Λ being the range of the potential (at $\xi = 2\Lambda$, $\Delta G_{PS-PS} = V = 0.07\ V_0$), and g^2 has the dimension of energy. The best fit curves of data with the MPT potential are shown in continuous lines in Figures 4d and 3c, and values of V_0 and Λ obtained from these fits are given in Table 1. From this table, it is clear that confinement has introduced an additional intermolecular potential whose magnitude, given by V_0, increases as film thickness is decreased but whose range remains more or less invariant. It should also be noted that for a film with thickness $>4R_g$ the in-plane potential is measurable but very small, which is consistent with the out-of-plane measurements. The situation is depicted in the cartoon in Figure 5.

We have seen from vuv spectroscopy that confinement of polystyrene beyond a thickness of $4R_g$ causes benzene dimers in the film to "lock" into a configuration with a near-zero dihedral angle. In particular, the reduction of the full width at half-maximum (fwhm) of the pure electronic band as the thickness is reduced from $4R_g$ onward indicates the emergence of a "superradiant" state of the dimers where the molecular transition dipoles are excited in-phase.[39] At the same time, we observe the emergence of a short-range repulsive intermolecular potential that has a strength increasing with confinement but whose range does not vary. We suggest that this new intermolecular force makes the polymer more "granular",[20] while the locked molecular configuration makes these "grains" more rigid, i.e., the lowering of intermolecular attraction is accompanied by an enhanced intramolecular (noncovalent) bonding.

Conclusion and Outlook

The measurements in this paper quantify the inter- and intramolecular interactions in nanoconfined polystyrene. Similar findings are expected in many substrate-supported polymer films, though the magnitude would be sample specific. We have found that, under one-dimensional nanoconfinement achieved simply through spin coating, atactic polystyrene becomes more ordered than the (inherently disordered) bulk polystyrene but is less cohesive. We show here that in aPS this phase is achieved through the alignment of adjacent benzene rings, explaining the similarity of confined aPS to the helically ordered phases of syndiotactic PS, as observed in infrared spectra.[13] This molecular rearrangement causes a new repulsive intermolecular potential to emerge.

Confinement-induced alignment of benzene rings is expected to cause polarization effects, and this expectation has indeed been borne out into a separate study of aPS films in the vacuum ultraviolet and will be reported soon. We have also found that the intermolecular repulsive potential in this nanoconfined material acts as a barrier that localizes excitons to the gyration spheres.[12] These potentials act as traps leading to tunable growth of monodisperse nanoparticles during diffusion of materials on polystyrene film surface.[25]

The contradictory properties of nanoconfined polystyrene may explain its other observed properties, such as the reduction of glass transition temperature (T_g) with confinement and its dependence on R_g and return to bulk T_g value on adding small-molecule diluents.[43] Also, the repulsive nature of the confinement-induced intermolecular potential can explain the phenomenon of reversible negative thermal expansion, observed in the polymer thin film.[44] The exact molecular mechanism involved in the reduction of cohesion on confinement may vary with the polymer involved and would be a subject of future research. Even for a particular polymer, the balance between entropic forces and interactions, which may get drastically modified due to confinement and lead to the decision of the dependence of cohesion on film thickness, itself depends on the molecular weight, and a systematic study of aPS of different molecular weights is of immense value.

References and Notes

(1) Cornil, J.; dos Santos, D. A.; Crispin, X.; Silbey, R.; Brédas, J. L. *J. Am. Chem. Soc.* **1998**, *120*, 1289.
(2) Chang, M. H.; Frampton, M. J.; Anderson, H. L.; Herz, L. M. *Phys. Rev. Lett.* **2007**, *98*, 027402.
(3) Beenken, W. J. D.; Pullerits, T. *J. Phys. Chem. B* **2004**, *108*, 6164.
(4) Tretiak, S.; Saxena, A.; Martinand, R. L.; Bishop, A. R. *Phys. Rev. Lett.* **2002**, *89*, 097402.
(5) Partridge, R. H. *J. Chem. Phys.* **1967**, *47*, 4223.
(6) Duke, C. B.; Fabish, T. J. *Phys. Rev. Lett.* **1976**, *37*, 1075.
(7) Duke, C. B.; Salaneck, W. R.; Fabish, T. J.; Ritsko, J. J.; Thomas, H. R.; Patton, A. *Phys. Rev. B* **1978**, *18*, 5717.

(8) Duke, C. B. *Mol. Cryst. Liq. Cryst.* **1979**, *50*, 63.
(9) Brédas, J. L.; Street, G. B. *J. Chem. Phys.* **1985**, *82*, 32.
(10) Furukawa, M.; Kato, H. S.; Taniguchi, M.; Kawai, T.; Hatsui, T.; Kosugi, N.; Yoshida, T.; Aida, M.; Kawai, M. *Phys. Rev. B* **2007**, *75*, 045119.
(11) Strobl, G. *The Physics of Polymers: Concepts for Understanding Their Structures and Behavior*; Springer: Berlin, 1997.
(12) Chattopadhyay, S.; Datta, A. *Phys. Rev. B* **2005**, *72*, 155418.
(13) Lupaşcu, V.; Picken, S. J.; Wübbenhorst, M. *Macromolecules* **2006**, *39*, 5152.
(14) Yanxiang, W.; Deyan, S. *Polym. Bull.* (*Berlin*) **1997**, *39*, 633.
(15) Uda, F.; Kaneko, F.; Kawaguchi, T. *Polymer* **2004**, *45*, 2221.
(16) Yu, C.-J. et al. *Phys. Rev. Lett.* **1999**, *82*, 2326; Zwanenburg, M. J. et al. *Phys. Rev. Lett.* **2000**, *85*, 5154; Donnelly, S. E.; et al. *Science* **2002**, *296*, 507.
(17) Sanyal, M. K.; Basu, J. K.; Datta, A.; Banerjee, S. *Europhys. Lett.* **1996**, *36*, 265.
(18) Seeck, O. H.; et al. *Europhys. Lett.* **2002**, *60*, 376.
(19) Doi, M.; Edwards, S. F. *The Theory of Polymer Dynamics*; Clarendon Press: Oxford, U.K., 1986.
(20) Demirel, A. L.; Granick, S. *J. Chem. Phys.* **2001**, *117*, 7745.
(21) Mukherjee, M. et al. *Phys. Rev. E* **2002**, *66*, 061801; Schuster, J.; Cichos, F.; von Borzcyskowski, C. *Eur. Polym. J.* **2004**, *40*, 993.
(22) Alcoutlabi, M.; McKenna, G. B. *J. Phys.: Condens. Matter* **2005**, *17*, R461.
(23) Patil, S.; Matei, G.; Oral, A.; Hoffmann, P. M. *Langmuir* **2006**, *22*, 6484.
(24) Sharma, A.; Mittal, J. *Phys. Rev. Lett.* **2002**, *89*, 186101.
(25) Chattopadhyay, S.; Datta, A. *Macromolecules* **2007**, *40*, 3313.
(26) Jérôme, B.; Commandeur, J. *Nature* **1997**, *386*, 589.
(27) Flügge, S. *Practical Quantum Mechanics*; Springer International Student Edition; Narosa Publishing House: New Delhi, 1979.
(28) Muthukumar, M. *Phys. Rev. Lett.* **2001**, *86*, 3188; Kong, C. Y.; Muthukumar, M. *J. Chem. Phys.* **2004**, *120*, 3460.
(29) Cacciuto, A.; Luijten, E. *Nano Lett.* **2006**, *6*, 901.
(30) Israelachvili, J. N. *Intermolecular and Surface Forces*; Academic Press: New York, 1992.
(31) Bower, D. I.; Maddams, W. F. *The vibrational spectroscopy of polymers*; Cambridge University Press: Cambridge, U.K., 1989; Hasegawa, T.; Nishijo, J.; Watanabe, M.; Umemura, J.; Ma, Y.; Sui, G.; Huo, Q.; Leblanc, R. M. *Langmuir* **2002**, *18*, 4758.
(32) Sinha, S. K.; Sirota, E. B.; Garoff, S.; Stanley, H. B. *Phys. Rev. B* **1988**, *38*, 2297.
(33) Tamayo, J.; Garcia, R. *Appl. Phys. Lett.* **1997**, *71*, 2394; Tamayo, J.; Garcia, R. *Appl. Phys. Lett.* **1998**, *73*, 2926.
(34) Schirmeisen, A.; Hölscher, H. *Phys. Rev. B* **2005**, *72*, 45431.
(35) Heim, L.-O.; Kappl, M.; Butt, H.-J. *Langmuir* **2004**, *20*, 2760.
(36) Bollinne, C. et al. *Eur. Phys. J. E* **2003**, *12*, 389.
(37) Nannarone, S.; et al. AIP Conference Proceedings 705; American Institute of Physics: New York, 2004; p 450; Pasquali, L. A.; Luisa, De; Nannarone, S. AIP Conference Proceedings 705; American Institute of Physics: New York, 2004; p 1142.
(38) Chattopadhyay, S.; Datta, A. *Chem. Phys. Lett.* **2004,** *391*, 216.
(39) Knoester, J. Proceedings of the International School of Physics, Organic Nanostructures: Science and Applications; IOS Press: Amsterdam, 2002; p 149.
(40) Pope, M.; Swenberg, C. E. *Electronic Processes In Organic Crystals*; Oxford University Press: New York, 1982.
(41) Janda, K. C.; et al. *J. Chem. Phys.* **1975**, *63*, 1419; Tsuzuki, S.; et al. *J. Chem. Phys.* **2002**, *117*, 11216.
(42) Cacace, M. G.; Landau, E. M.; Ramsden, J. J. *Q. Rev. Biophys.* **1997**, *30*, 241.
(43) Forrest, J. A.; Dalnoki-Veress, K.; Stevens, J. R.; Dutcher, J. R. *Phys. Rev. Lett.* **1996**, *77*, 2002; Ellison, C. J.; Ruszkowski, R. L.; Fredin, N. J.; Torkelson, J. M. *Phys. Rev. Lett.* **2004**, *92*, 095702.
(44) Mukherjee, M.; Bhattacharya, M.; Sanyal, M. K.; Geue, T.; Grenzer, J.; Pietsch, U. *Phys. Rev. E* **2002**, *66*, 061801.

MA071392Y